Palaeontology
The Palaeontological Association
www.palass.org

[Palaeontology, Vol. 64, Part 2, 2021, pp. 179–202]

COMPARING SURFACE DIGITIZATION TECHNIQUES IN PALAEONTOLOGY USING VISUAL PERCEPTUAL METRICS AND DISTANCE COMPUTATIONS BETWEEN 3D MESHES

by VERÓNICA DÍEZ DÍAZ[1,2], HEINRICH MALLISON[3,4], PATRICK ASBACH[5], DANIELA SCHWARZ[1] *and* ALEJANDRO BLANCO[6,7]

[1]Museum für Naturkunde, Leibniz-Institut für Evolutions-und Biodiversitätsforschung, Invalidenstraße 43, 10115 Berlin, Germany; diezdiaz.veronica@gmail.com, daniela.schwarz@mfn.berlin
[2]Humboldt Universität, Berlin, Germany
[3]CeNak Hamburg, Hamburg, Germany; mallison@palaeo3d.com
[4]Palaeo3D, Pöttmes, Germany
[5]Department of Radiology, Charité – Universitätsmedizin Berlin, Corporate member of Freie Universität Berlin, Humboldt-Universität zu Berlin, and Berlin Institute of Health, 10117 Berlin, Germany; patrick.asbach@charite.de
[6]Centro de Investigacións Científicas Avanzadas (CICA), Facultade de Ciencias, Universidade da Coruña, 15071 A Coruña, Spain; alejandro.blancoc@udc.es
[7]Bayerische Staatssammlung für Paläontologie und Geologie, Richard-Wagner-Str. 10, 80333 München, Germany

Typescript received 9 July 2020; accepted in revised form 5 November 2020

Abstract: The use of surface digitization techniques and methods in palaeontology has increased in the last two decades, mainly due to recent improvements in devices and software. However, many digitization efforts are published only as 3D models, with only a few details on the exact protocols used and sometimes not even indicating how to access these digital data, thus reducing the long-term reusability of the obtained files. It is important to include this information, as the applied techniques and workflows have significant effects on the final quality of 3D models. We compare 3D meshes created by seven different surface digitization techniques and protocols for a sauropod caudal vertebra and a testudine turtle in a flat slab of rock. These two specimens represent typical examples of objects in vertebrate palaeontology collections, making them a suitable sample for our tests. Besides these quantitative and topological comparisons we also have computed visual perceptual metrics, which aim to predict the visual quality of a 3D model as perceived by a human observer. Our results agree with previous works, confirming that photogrammetry is one of the most suitable options for obtaining high quality 3D models of fossils, producing higher quality meshes than current structured light 3D scanners.

Key words: surface digitization, vertebrate palaeontology, 3D model, photogrammetry, structured light 3D scanning, visual perceptual metrics.

SURFACE digitization has greatly contributed to the preservation and documentation of palaeontological and zooarchaeological sites and remains since the last decades of the twentieth century. These efforts are most evident in the documentation of ichnological sites (Baltsavias 1999; Breithaupt *et al.* 2001, 2004; Matthews *et al.* 2006, 2016; Bates *et al.* 2008, 2009). These preservation works normally combine several digitization techniques to gather as much information as possible; for example, close-range photogrammetry and airborne laser scanners such as LiDAR (light detection and range laser scanner), which is a highly accurate and fast method of acquiring 3D spatial data (Bates *et al.* 2008). Other available devices and methods include short-range laser scanners, geographic information systems (GIS), low-altitude remote-controlled airplane (LARCA) with a camera and an aerial camera blimp system (ACBS) for aerial photographic documentation, all of which add more data to the information that can be extracted from the site (Breithaupt *et al.* 2004; Matthews *et al.* 2006; Bates *et al.* 2009). All these works also provide useful tips for the correct digitization of trace fossils (for photogrammetry, see e.g. Breithaupt *et al.* 2004; Matthews *et al.* 2016).

Surface digitization of isolated palaeontological, anthropological and zooarchaeological remains has been more systematically developed since the beginning of the

doi: 10.1111/pala.12518

twenty-first century. Several authors have already investigated which methods are more reliable for digitizing isolated specimens, normally focusing on computed tomography (CT) scanners (clinical or microCT scanners), white light scanners and close-range photogrammetry (hereafter referred to as photogrammetry). For example, studies comparing microCT scans to 3D surface scans have become more abundant relative to other methods (e.g. Slizewski *et al.* 2010; Robinson & Terhune 2017; Marcy *et al.* 2018). More specifically, Lautenschlager (2016), Fahlke & Autenrieth (2016) and Hamm *et al.* (2018) compared the 3D outputs created by photogrammetry and CT scanners. Katz & Friess (2014), Evin *et al.* (2016) and Fau *et al.* (2016) compared 3D models created by photogrammetry and a light scanner, while Giacomini *et al.* (2019) compared the results obtained by these two techniques and CT scanning. Some of these works have also included time values (for data acquisition and processing of data) to additionally test the efficiency of the methods. For comparison, most works relied on geometric morphometric approaches and analyses of variance (ANOVA). In summary, photogrammetry seems to be a reliable method for obtaining high quality surface 3D models, while laser and structured light 3D scanners seem to be more efficient (although the created meshes do not normally present the same quality as the ones created by photogrammetry). For example, photogrammetry has proved to be as accurate as manual measurements in generating landmark-based 3D morphometric data (Muñoz-Muñoz *et al.* 2016; Bastir *et al.* 2019; Giacomini *et al.* 2019; Tsuboi *et al.* 2020). Bastir *et al.* (2019) and Peterson & Krippner (2019) went one step further, also assessing the quality of the 3D printed models created by some of these digitization techniques. Besides these comparative analyses, other authors have also provided useful analyses of digitization workflows for palaeontological specimens (see e.g. Falkingham 2012; Mallison & Wings 2014).

However, apart from these statistical and landmark-based analyses, no other mesh quality definitions and indicators are normally detailed. Furthermore, visual comparisons between meshes (when carried out) are based on personal observations (see e.g. Evin *et al.* 2016); not only could the results of these be very subjective, but they could depend on several factors (e.g. visual system of the observer, media used to visualize the mesh, or the environmental conditions; Corsini *et al.* 2012).

In this work, we assess the quality of several 3D models of two fossil specimen types that can easily be found in a vertebrate palaeontology collection: a sauropod dinosaur caudal vertebra and a testudine turtle in a slab of rock. Both specimens have been digitized using a structured light 3D scanner and different photogrammetry protocols. Mesh quality indicators are used to better compare the quality of the meshes, together with topological and quantitative comparative methods (i.e. distance computations), and visual perceptual quality metrics. These metrics provide more accurate and reliable results for qualitative visual comparisons, and have not been previously used in comparative analyses in palaeontology or zooarchaeology. This work will for the first time assess their validity in these fields.

VISUAL PERCEPTUAL METRICS

Understanding human perception and cognition, as well as modelling human visual system (HVS) behaviour is an essential step for developing image-based applications (Wandel 1995). HVS perceives a stimulus depending on its colour/intensity, orientation, and also spatial distribution. That is why visual aspects such as masking and saliency have been explored and studied, especially when analysing the quality of 2D and 3D meshes (Corsini *et al.* 2012).

The research on objective mesh visual quality (MVQ) assessment is still in its early stages, but several perceptual metrics have already been proposed in the last decade for assessing the subjective visual quality (or visual impact distortion) of a static 3D mesh with respect to a reference model (see e.g. Lavoué & Corsini 2010; Lavoué 2011; Corsini *et al.* 2012; Feng *et al.* 2018). A metric is a function of pairs of images that gives a non-negative measure of the distance between two images (Lindstrom & Turk 2000). These metrics can be separated in two categories, discussed below.

Image-based metrics

These metrics apply the perceptual mechanisms of the HVS to a still image generated from the 3D data using rendering techniques; they are thus view-dependent. They are evaluated on the basis of a set of images created from different views of the 3D object. But this approach is not completely reliable, as the visual perception of a set of images of a certain 3D object is different from that perceived by a human observer of the 3D model in a graphics application (Rogowitz & Rushmeier 2001). In addition, depending on the medium, colour does not always seem similar (Corsini *et al.* 2012). The perception of a colour stimulus is partly dependent on the environment's properties, such as background colour and lighting conditions.

Geometry-based metrics

These metrics analyse the geometry of the 3D models to predict perceptual impairments or evaluate other perceptual quality aspects, making the evaluation view-

independent. There are two types: classical geometric metrics and model-based metrics. The first have a poor correlation with human visual perception. In contrast, model-based metrics are perception-aware and have a significantly higher correlation with human visual perception. This perceptual quality refers to the quality that is produced by a perception-aware metric.

Geometry-based perceptual metrics aim to predict the visual quality of a 3D model as perceived by a human observer. This perceived quality can also be directly and quantitatively assessed by means of subjective tests, in which human observers directly provide ratings about the perceived quality of several distorted models. A mean opinion score (MOS) is then computed for each distorted object, reflecting its average quality as assessed by the observers. Several studies have confirmed the good correlation between subjective tests and objective metrics (Rogowitz & Rushmeier 2001; Corsini *et al.* 2012; Feng *et al.* 2018) so we relied on perceptual metrics in our study; more specifically, model-based ones. We computed one of the most used MVQ metrics, the Mesh Structural Distortion Measure 2 (MSDM2) described by Lavoué (2011), which has one of the highest correlation values with MOS. As stated by Lavoué (2011, p. 1): 'this approach first computes a fast asymmetric matching between the distorted object and the original one, then for each vertex, Gaussian-weighted curvature statistics are computed at multiple scales over local windows to produce a local distortion map; local values are then pooled into a single Global Multiscale Distortion score (GMD). The final metric is obtained by averaging forward and backward global distortion scores', meaning that this metric is symmetrical, obtaining the same score independently of the mesh used as a reference. This measure relies on differences of structure (captured via curvature statistics) computed on local corresponding neighbourhoods from the meshes being compared. In addition, and as previously confirmed by Zhu *et al.* (2010), the perceptability of a distortion on a 3D object depends on its level of detail and its viewing conditions (e.g. display resolution and viewing distance), so the MSDM2 depends on three scale parameters. This increases its efficiency and robustness. This metric scales non-linearly from 0–1: a value of 0 means that the two objects are identical while values near 1 indicate that they are visually very different. However, this metric requires calibration (see below).

These visual perceptual metrics are largely used in computer graphics for assessing the quality of 3D meshes, in order that they do not appear to be degraded to a human observer. The objective is to find the minimum representation of a 3D object that does not compromise the visual quality of the object when it is rendered in two dimensions (Rogowitz & Rushmeier 2001). We included these metrics in our comparison sets as the MVQ is also important in palaeontology: as stated above, on most occasions, 3D models are the sole data used for scientific research, with many researchers never accessing the original specimens. In some studies, researchers use these 3D models to describe physical features of the specimen (using their own HVS; e.g. for phylogenetic analyses, landmark coordinates or musculoskeletal reconstructions) and the application of these visual perceptual metrics for assessing the best 3D models prior to conducting such research could be of great assistance.

NOTES ON TERMINOLOGY AND CYBERTAXONOMY

Accessibility of the digital data

Recent improvements in the quality of digital cameras and photogrammetry software combined with an increase in the level of generally available computing power have led to a dramatic expansion of specimen surface digitization in many sciences. Already suggested as the method of choice for practically all surface digitization attempts by Sutton *et al.* (2014), photogrammetry has become the current gold standard for surface-based digitization methods (Hamm *et al.* 2018), matching the ubiquity and accuracy of CT scanning for specimens where internal features are of primary interest. At the same time, laser and structured light 3D scanning have also become more commonly used, with hand-held scanners allowing costefficien and rapid high resolution digitizing.

This surge in digitizing has already produced a number of easily accessible virtual collections (e.g. DigiMorph, http://digimorph.org; MorphoSource, https://www.morphosource.org; Open Science Framework: https://osf.io/ecmz4/wiki/home; Digital Fish Library, http://www.digitalfishlibrary.org; Berquist *et al.* 2012) along with published descriptions of data capture and modelling protocols (e.g. Falkingham 2012; Mallison & Wings 2014; Lautenschlager 2016). However, some digitization efforts are published as their finished 3D models (primarily the use for meshes created by surface digitization techniques) with only a few details on the exact protocols used (especially post/processing workflows) or indications of how to access the digital files (including raw data), reducing the long term reusability of the assets produced (see e.g. Davies *et al.* (2017) and Falkingham *et al.* (2018) for the type of data that should be included with the final 3D files). For example, in some cases data were obtained, but are only available on request (see e.g. Mallison 2010; Tsuboi *et al.* 2020), in other works the scans, or only part of the digital material, were published in low-resolution with no high resolution or raw data available via an institution (see e.g.

Cerroni *et al.* 2020; Ibrahim *et al.* 2020) but in most cases the published works do not include any information on how to access these digital data (see e.g. Vidal & Díez Díaz 2017; Vidal *et al.* 2020). Often, the raw data underlying the model can be obtained, especially if the user makes them available (e.g. as supplementary data), but the details of how the model was extracted, especially of any manual editing, are often omitted. Such manual or automated editing of data (also known as post-processing), including simplifications for the purpose of reducing file size, are important aspects in addition to the pure data capture and model analysis routines. In this context, it is important to differentiate between 'digitization' and 'edition'. The term 'digitization' (also known as processing protocol) is defined as the process in which a digital representation of a fossil specimen is created from its physical analogue using an analogue-to-digital converter (e.g. a scanner or a camera). Normally, this process should present little user interference (depending on the technique used, as this work will show), contrasting with the process of 'edition' (also known as post-processing protocol), in which the user manipulates the initial data, modifying it according to the final desired quality and use of the 3D model (e.g. by eliminating errors, closing holes, decimating, or modelling the mesh).

Cybertypes in biological and palaeontological sciences

When a researcher cannot directly access an original specimen, they will usually consult published photographs, interpretive drawings and descriptions. However, 3D files are increasingly becoming the main data used for scientific research when access to the physical specimen is not possible. Indeed, physical specimens can deteriorate, break or disappear due to natural causes, but also through handling or the use of destructive techniques (e.g. the serial grinding methodology used to digitally visualize and 3D reconstruct the Silurian fauna of Herefordshire, Sutton *et al.* 2001*a*, *b*; Siveter *et al.* 2020). In such cases, it can be argued that the virtual model could become a 'digital specimen' in its own right. Various terms have been suggested for such cases. The term 'cybertype' was first used by Godfray (2007 page 260) and defined as 'a new form of type specimen . . . to be displayed on the web using the very best current imaging methods — often far superior to normal examination — . . .'. Adams *et al.* (2010, p. 5) proposed the term 'digitype', defining it as the 'digital equivalent of a plastotype'. Faulwetter *et al.* (2013) provided a more detailed definition of such virtual type material, stating that most of the recently created datasets might not qualify for the notion of a cybertype, as in most studies the 3D models were digitized with a specific use in mind so the resulting data were not useful for other purposes (e.g. generally, meshes used in finite element analyses (FEA) are not suitable for detailed anatomical descriptions). So, datasets that are intended to serve as a cybertype should fulfil at least the following three basic assumptions (Faulwetter *et al.* 2013):

1. It should provide morphological and anatomical information of the same accuracy and reliability as that provided by the physical type material, independent of any specific given research question.
2. It should be linked to the original type material, which can be consulted if in doubt. This implies that any method used to create the cybertype should not affect the morphological, anatomical or molecular identity of the original specimen (e.g. holotype, paratype or neotype).
3. It has to be retrievable and freely accessible. This involves making the data available via a reliable (internet) source under an open access licence and providing adequate security measures, such as archiving, backups and future-proofing by ensuring forward compatibility of data format, and allowing the annotation of the dataset with metadata in order for it to be retrievable and interpretable.

The term 'cybertype' and its use have been already discussed in the recent literature and at a number of biological scientific meetings (Akkari *et al.* 2015). These authors state 'as a supplement to the biological material, a cybertype adds value to the material collections and facilitates sharing of primary biodiversity data, reducing the reliance on handling of physical specimens to allow a new species to be included in more research efforts' (Akkari *et al.* 2015, p. 20). More data can be included within the cybertype besides the 3D model of the physical specimen, such as a full transcriptome, a DNA barcode, a movie of the living animal, and a microCT image of a paratype, as Stoev *et al.* (2013) did when describing a new species of a cave-dwelling centipede. Although more discussion is needed on this nomenclature of digital types, we suggest also using 'cybertype' in palaeontology as a digital synonym of 'holotype' (as it is more extensively described than a digitype), and 'digitype' as a digital synonym of 'paratype'.

Almost all the 3D models created in this project fulfil the three criteria mentioned by Faulwetter *et al.* (2013), also including all the essential (for verification) and recommended (as best practice) data files suggested by Davies *et al.* (2017), so they can be considered as cybertypes. However, only one digitized 3D model per specimen will be considered as such, after the discussion of the quality of the final mesh and appropriateness of the technique, method and workflow. The rest of the created meshes will be considered as digitypes, and included as supplementary data within each cybertype.

Mesh quality indicators

Some studies (e.g. Gonizi Barsanti & Guidi 2013) have defined mesh quality in relation to the detail and accuracy of the mesh geometry. Ramos Barbero & Santos Ureta (2011) went further, detailing several indicators to test the quality of the created meshes:

1. Accuracy of the digitization device and the mesh (by using calibrated pieces).
2. Distribution of points and quality of the mesh distribution (from very rough surfaces with many holes to smooth surfaces without holes).
3. Mesh of edges.
4. Holes without meshing.
5. Part digitization.

Knupp (2007, p. 2) stated that 'Mesh Quality concerns the characteristics of a mesh that permit a particular numerical [partial differential equations] simulation to be efficiently performed, with fidelity to the underlying physics, and with the accuracy required for the problem. ... mesh quality depends on the particular calculation which is undertaken and thus changes if a different calculation is performed. ... a mesh should ... not create difficulties for the simulation. ... the mesh should result in sufficiently accurate simulations, i.e., those which are in the asymptotic regime, and those which reduce both global and local error below the required level. Ultimately, the mesh and discretization method together must enable the simulation to satisfy the requirement that the size of the error bars due to problem discretization are acceptable.' In this work, we determined the quality of the digitized meshes taking into account several mesh features and quality indicators:

1. Resolution: number of vertices.
2. Quality of triangulation: the more equilateral the triangles, the better is the triangulation.
3. Number of topological artefacts: i.e. errors, holes, non-manifold parts.
4. Quantitative comparison (differences between the number of vertices, mesh area and volume, mean distance and standard deviation) with its edited mesh (i.e. of higher quality, as the holes were closed and the errors eliminated). Mean distance and standard deviation values were calculated after a 'cloud-to-mesh distances' computation, in which the software (in our work CloudCompare) will simply search the nearest triangle in the reference mesh for each point of the compared cloud (see below).
5. Accuracy: the difference between a target position in the mesh and the actual position in the physical specimen. Scale bars were used for measuring the accuracy in the photogrammetric methods, so that the scaling error could be calculated in the processing protocol. The mean error was calculated for the meshes created with structured light 3D scanners, as each scan had a scaling error.

However, it is important to note that mesh quality is not a uniform metric depending on the required function of the model. Indeed, as indicated by Knupp (2007), the quality will depend on the particular use for which the mesh has been created. Mesh quality for computational analyses (e.g. for FEA isometric elements, a certain resolution may be required) is not necessarily comparable to that for 3D anatomical models. Anatomical models can accommodate differently sized elements to achieve the necessary topology while keeping the number of elements to a minimum. That is why this work gathers together the above mentioned mesh quality quantitative indicators with topological and visual qualitative comparative analyses (i.e. visual perceptual metrics).

Institutional abbreviation. MB.R., Museum für Naturkunde Berlin, Germany.

Digitization technique abbreviations. C2M, cloud-to-mesh distances; CT, computed tomography scanning; TT10, turntable method (10°) with the Canon EOS 70D DSLR camera; TT10HQ, turntable method (10°) with the Canon EOS 5DS R DSLR camera; TT30, turntable method (30°) with the Canon EOS 70D DSLR camera; TT30HQ, turntable method (30°) with the Canon EOS 5DS R DSLR camera; WAM, photogrammetry 'walk-around method'.

HYPOTHESES

The main hypotheses to test were whether the methodology, digitization technique or device used interfered with the quality of the final 3D model. See Devices for Data Acquisition, Data Acquisition Protocols, and Processing Protocols, below, for more detailed descriptions of the devices and workflows used. Further specific issues were tested to address these hypotheses:

1. For photogrammetry, two different sets of camera equipment and data capture protocols were tested, to determine whether the final quality of the 3D model is highly dependent on the quality of the camera equipment. The Canon EOS 5DS R DSLR (50.6 MP) camera provides substantially higher image quality than the Canon EOS 70D (20.2 MP), as do the lens and ring flash used with the former. However, the Canon EOS 5DS R DSLR camera presents a smaller depth of field, and this may affect the alignment of the photographs, as photogrammetry software calculates focal points and searches for equal points between photographs. For both sets of camera

equipment, an ISO of 800 was used, as it was considered to be an upper limit for obtaining good photographs with little noise for the correct calculation of points in alignment (although ISO value and noise is highly camera-dependent).
2. For the turntable method we wanted to assess whether the quality of the mesh was highly dependent on the number of photographs.
3. As the Artec Space Spider scanner offers a higher resolution than the Artec Eva scanner (500 μm vs 100 μm) we expected the former to create better quality 3D models than the latter. We also digitized the specimen MB.R.3642 twice with the Artec Eva scanner, creating one mesh with six scans and the other with only one scan; the hypothesis here being to test whether the number of scans highly affects the final quality of the 3D model.
4. Finally, we wished to determine if there were marked contrasts in quality between photogrammetry-based and structured light 3D scan meshes.

FOSSIL SPECIMENS

Because of the preservation, size and object complexity (i.e. ridges, rugosities, concavities etc.) we selected a caudal vertebra (MB.R.2091.19, twelfth in the series) (Fig. 1) of the mamenchisaurid sauropod *Wamweracaudia keranjei*, from the Upper Jurassic Tendaguru Formation (Tanzania) (see Mannion *et al.* 2019 for a more detailed anatomical description of this specimen) (Heumann *et al.* 2018). This caudal vertebra is easy to handle because of its preservation and size (centrum length: 12.5 cm, vertebral height: 29 cm, posterior articular surface width: 13.8 cm) and its shape is not very complex, suitable for testing a simple digitizing protocol. As a second specimen, we selected the testudine turtle *Araripemys barretoi* (MB.R.3642), from the Lower Cretaceous Araripe Basin (Brazil) (Price 1973) (Fig. 2). This specimen, preserved as a relief of its ventral surface on a slab of rock (19 cm × 33 cm × 21.7 cm), offers a greater challenge due to its uniformity of colour, the occurrence of slight undercuts, and overall much finer detail. These two specimens represent typical examples for objects in vertebrate palaeontological collections (one of them more spherical, and the other embedded in sediment and predominantly flat), making them a suitable sample for our tests.

DEVICES FOR DATA ACQUISITION

To investigate different techniques for 3D model reconstruction different methods and post-processing tools were included in this study (Table 1):

Photogrammetry

Besides the camera equipment detailed in Table 1, we also used a tripod Manfrotto 190 and a Manfrotto MHXPRO 3-way head, a turntable marked with degrees (photographs were shot at both 10° and 30°), and accurate scale bars with coded targets recognized by several pieces of photogrammetry software (two two-point scales (0.1 and 0.25 m) and one three-point scale (0.25 m) placed around MB.R.2091.19, and two two-point scales (0.1 m) and one three-point scale (0.25 m) placed around MB.R.3642). The use of ring flashes gave us more controlled light conditions, allowing us to get closer to the specimens with a good depth of field value at short exposures.

Structured light 3D scanning

Artec Eva scanner (100 μm resolution); Artec Space Spider scanner (500 μm resolution).

DATA ACQUISITION PROTOCOLS

Photogrammetry

MB.R.2091.19 specimen. Two sets of photographs were taken for each method (each with a different fabric background (blue or green) if subsequent masking was needed). Scale bars were placed in one of the sets, for subsequent scaling of the 3D model. For each set, five general photographs were taken, with all scale bars visible (in the relevant set): each side of the specimen from above, and completely perpendicular to it (Fig. 3). In this way, the general morphology of the specimen was captured, together with the complete scale bars.

MB.R.3642 specimen. As only one surface of the specimen was going to be digitized, no fabric backgrounds were used, and only one set of photographs was taken. Five general photographs with visible scale bars were taken. This led to a post-cleaning of the background for creating better comparison analyses and values (see below).

Walk-around method. (Also known as manual photogrammetry.) For this photoset we followed the methodology proposed by Mallison & Wings (2014, p. 9): 'Move the camera in relation to the specimen (or vice versa) to create parallax... Each point on the specimen must be well visible and in focus on at least two images. ... Take photographs with 40-60% overlap... Avoid near-identical photographs...'. The ideal situation would be that every

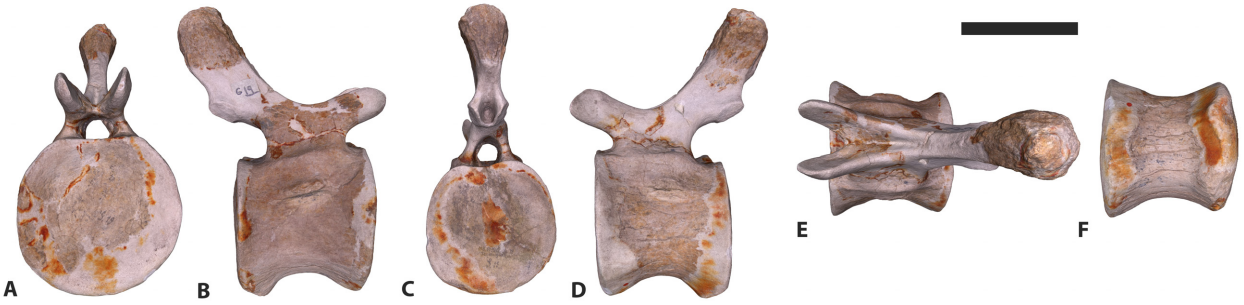

FIG 1. MB.R.2091.19, caudal vertebra (12th in the series) of the mamenchisaurid sauropod *Wamweracaudia keranjei*, from the Upper Jurassic Tendaguru Formation (Tanzania) in: A, anterior; B, right lateral; C, posterior; D, left lateral; E, dorsal; F, ventral view. Set of images from the chosen cybertype (MB_R_2091_19_WAM) for this specimen. Scale bar represents 10 cm.

FIG 2. MB.R.3642, testudine *Araripemys barretoi*, from the Lower Cretaceous Araripe Basin (Brazil). Image from the chosen cybertype (MB_R_3642_TT30HQ) for this specimen. Scale bar represents 5 cm.

point appears on average in four photographs, three at the minimum, five at most. The use of too much raw data should be avoided.

Turntable method. We followed here the same guidelines proposed by Mallison & Wings (2014), with the camera on a tripod and rotating the turntable by 10° and 30° between shots. 'The photograph series thus forms a perfect circle of camera positions around the specimen, with the camera always aimed at the central vertical axis of the turntable.' For specimen MB.R.2091.19 we took three concentric circles of photographs at different heights, to cover all of its surface.

We highly recommend the works of Falkingham (2012), Mallison & Wings (2014) and Matthews *et al.* (2016) for more detailed workflows and tips on how to create high quality 3D models of fossil specimens, skeletal mounts and ichnological sites (also applicable to 'flat' specimens, or those embedded in slabs of rock) using photogrammetry.

Structured light 3D scanning

The methodology used with both scanners was the same, differing only in scanning distance (the Artec Eva scanner can scan from a distance of between 0.4 and 1 m; the Artec Space Spider scanner between 0.2 and 0.3 m). The specimen was placed on a turntable and the scanner held by the user. The turntable was then rotated slowly, while the scanner was held still or moved slightly to capture all of the specimen's surface. MB.R.2091.19 was turned for scanning the posterior surface (i.e. several scanning sets were created). The scans were made at 7–8 frames per second, with the 'real-time fusion' option enabled. Besides the general scans, more detailed sets (getting closer, or scanning from different directions) were made focusing on the more complex regions of the specimen (e.g. the neural arch and spine). Both specimens were easily scanned with the Artec Eva scanner, but the process was more difficult to follow with the Artec Space Spider scanner, probably due to the specimens' sizes, meaning that these objects probably reach the size limit that this scanner can be used for. The laptop used for both scanners has an Intel® Core™ i7-6820HQ Processor at 2.70 GHz, with 64 GB of RAM and a NVIDIA Quadro M5000M graphics card.

TABLE 1. Digitization methods and equipment tested in this work.

Method abbreviation	Method	Turntable degrees	Camera/scanner	Resolution	Lens	LED ring flash	Camera mode	Aperture value	ISO	3D model file name
WAM	Walk-around method	–	Canon EOS 70D	20.2 MP	Canon EF-S 10–18 mm f/4.5-5.6 IS STM	Non-professional LED ring flash	AV	f/5.6	800	MB_R_2091_19_WAM MB_R_3642_WAM
TT10	Turn-table method	10°	Canon EOS 70D	20.2 MP	Canon EF-S 10–18 mm f/4.5-5.6 IS STM	Non-professional LED ring flash	AV	f/5.6	800	MB_R_2091_19_10 MB_R_3642_10
TT30		30°								MB_R_2091_19_30 MB_R_2091_19_30HQ
TT10HQ		10°	Canon EOS 5DS R	50.6 MP	Canon EF 50 mm f/2.5 Compact Macro	Canon Macro Ring Lite MR-14EX	M	f/8	800	MB_R_2091_19_10HQ MB_R_3642_10HQ
TT30HQ		30°								MB_R_2091_19_30HQ MB_R_3642_30HQ
EVA	Structured light 3D scanning	–	Artec Eva	100 µm	–	–	–	–	–	MB_R_2091_19_EVA MB_R_3642_EVA_1Scan MB_R_3642_EVA_6Scans
SPIDER		–	Artec Space Spider	500 µm	–	–	–	–	–	MB_R_2091_19_SPIDER MB_R_3642_SPIDER

Camera mode: AV, aperture priority; M, manual exposure.

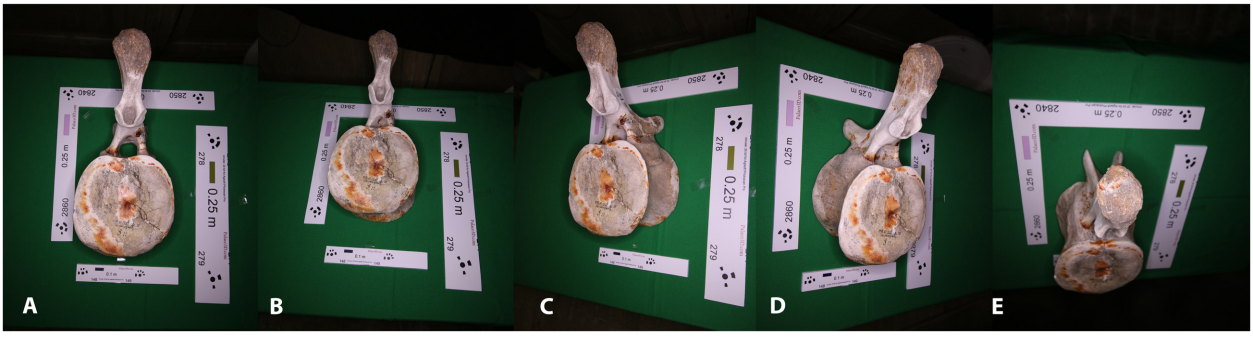

FIG 3. For each photogrammetry set, five general photographs were taken with all scale bars visible (if included in the set). Photographs of MB.R.2091.19: A, completely perpendicular to the specimen; B–E, each side of the specimen from above: B, ventral; C, right; D, left; E, dorsal view.

PROCESSING PROTOCOLS

Production of the 3D meshes

Following the recommendations of Davies *et al.* (2017), essential (for verification) and recommended (as best practice) data files were created for each 3D model: final 3D models (STL file, which is simple and supported by the vast majority of 3D visualization programs; Sutton *et al.* 2014), as well as OBJ files with texture information (as JPG), text file (with description of scanner settings or how the images were acquired, resolution, techniques used to produce the 3D model, specimen information etc.) and original capture data (photographs or data acquired by scanner). All of these files are stored at the Museum für Naturkunde (Díez Díaz *et al.* 2020).

Photogrammetry. The computer used for the creation of the 3D models has an Intel® Core™ i7-6700HQ Processor at 2.60 GHz, with 16 GB of RAM, a NVIDIA GeForce GTX 965M graphics card, a 256 GB SSD, and a 1 TB HDD (programs and data were run from the SSD). There are numerous pieces of commercial and free photogrammetry software, but for consistency we only used Agisoft Metashape Pro (v. 1.5.5) (https://www.agisoft.com) in this work. The workflow followed is mainly the one proposed by Mallison *et al.* (2017). All photograph sets were grouped in one block, with the exception of the ones created for MB.R.2091.19 by the TT10HQ and TT30HQ methods (see below). The face count was set to zero, to obtain the maximum number of faces when building the mesh.

New sets of detailed photographs made by the user had to be included in the previous MB.R.2091.19 sets made with the Canon EOS 70D DSLR camera and the turntable method (TT10 and TT30 methods), as the neural arches were not sufficiently digitized in the first attempts (probably because the combination of turntable method with this camera and/or lens did not allow for the proper capture of the more complex surfaces; e.g. with more depth, ridges, details). These surfaces were not sufficiently digitized as the user did not manually focus the camera, in order to test an 'almost entirely automated' process. However, we needed to include these new sets of photographs so that the meshes had the necessary quality to be used in the comparisons.

The photographs made with the Canon EOS 5DS R DSLR camera for creating the TT10HQ and TT30HQ meshes of MB.R.2091.19 had to be separated into two blocks and masked, as the initial alignments were insufficient to follow the general workflow (i.e. the software did not align both sets of photographs when they were in the same block). Later, both blocks were merged using markers, and the final 3D model was created following the general workflow with the merged block. For the MB.R.3642 mesh created with the TT30HQ method only 35 photographs were aligned, probably as a result of the software having difficulty in calculating shared points due to the depth of field of the camera, and the smaller number of photographs (with less overlap between them).

Structured light 3D scanning. We used the Artec scanners' bespoke software for 3D scanning and data processing: Artec Studio 13 Professional. With the 'Editor' tool the scans were cleaned, and later aligned with the 'Align' tool. After alignment, frames with more than 10 errors were deleted from the scans (with the exception of the frames that had texture information). In the 'Tools' section, the 'Global Registration' tool was run. With this final 3D mesh we obtained the texture, and then exported the files to STL and OBJ.

Although it is possible to close the holes present in the mesh with the software Artec Studio 13 Professional, we decided to follow the post-processing protocol with the software GOM Inspect (see below) used for the meshes created with photogrammetry. The algorithms used by

each software for searching and closing the holes are not the same, and we tried to standardize the workflows as much as possible for retrospective comparisons.

POST-PROCESSING PROTOCOLS

Preparation of STL files for retrospective comparison

We analysed the resulting STL files looking for errors (see Table 2) with the software GOM Inspect. This software can detect topological errors in the 3D mesh, such as holes, sewing errors (when two mesh areas are not connected to each other), intersections (when at least one triangle penetrates another one), fanfolded triangles (triangles that partly lie on top of each other and are connected to each other on at least one side), erratic points (when two holes touch each other) and degenerated triangles (when they are too narrow). Errors were eliminated and holes closed for creating the edited meshes (considered to be of higher quality than the digitized ones, as no topological artefacts were present). However, only the digitized meshes were used for the quantitative, topological and visual comparisons (see below), because they are the original outputs of each digitization method.

As the final resolution of the 3D mesh is highly dependent on the user's influence we decided not to edit the holes inside the neural canal, and let the software GOM inspect close them using the 'Close Holes > Automatically' algorithm. After using this algorithm the neural canal was completely closed in these meshes, creating new points. As this is an artefact, this section cannot be used in the comparative analysis (see below).

Non-manifold edges and vertices, the quality of the triangulation (mean ratio of the triangles), and the mesh surface area and volume were calculated with the software MeshLab v.2106.12 (https://github.com/cnr-isti-vclab/meshlab/releases/tag/v2016.12) (Tables 2–4).

As previously noted, the background of the MB.R.3642 meshes needed to be cleaned, as scale bars were visible in some of them. The faces of the mesh that were not close to the fossil bones were eliminated with the software GOM Inspect (GOM software 2018; https://www.gom.com/3d-software/gom-inspect.html). The scale of the meshes created with the Artec scanners was different to the meshes created with photogrammetry (the former were 100 times larger), so they were scaled beforehand with the same piece of software.

VISUAL PERCEPTUAL METRICS

The MSDM2 metric was computed in the 3D Mesh Processing Platform MEPP (https://projet.liris.cnrs.fr/mepp;

TABLE 2. Computed errors of each mesh uisng GOM Inspect and Meshlab.

3D model file name	Holes	Sewing errors		Intersections (triangles)	Fanfolded triangles	Erratic points	Non-manifold edges	Non-manifold vertices	Degenerated triangles	% Degenerated triangles
MB_R_2091_19_WAM	0	0		113	1	0	0	0	472 749	2.67
MB_R_2091_19_10	1	0		97	1	0	0	0	458 003	2.71
MB_R_2091_19_30	2	0		9	0	0	0	0	571 682	3.38
MB_R_2091_19_10HQ	2	0		249	12	0	3V; 6F*	0	1 053 187	3.16
MB_R_2091_19_30HQ	2	0		86	13	0	0	0	945 785	3.04
MB_R_2091_19_EVA	356	3		0	0	130	0	130	6497	0.49
MB_R_2091_19_SPIDER	202	8		0	0	51	0	51	8500	0.62
MB_R_3642_WAM	2	1		87	0	1	0	1	191 025	2.16
MB_R_3642_10	4	2		26	0	3	0	3	92 526	2.12
MB_R_3642_30	5	2		23	0	3	0	3	88 136	2.11
MB_R_3642_10HQ	1	2		211	1	0	0	0	229 346	2.13
MB_R_3642_30HQ	2	2		206	2	1	0	0	216 424	2.12
MB_R_3642_EVA_1Scan	14	0		0	0	2	0	2	2256	0.71
MB_R_3642_EVA_6Scans	13	0		0	0	0	0	0	2172	0.68
MB_R_3642_SPIDER	60	0		0	0	5	0	5	1776	0.56

*V, vertices; F, faces

TABLE 3. Data on the triangulation quality of each mesh.

3D model file name	Mean	Median	Standard deviation	Variance
MB_R_2091_19_WAM	0.721946	0.855873	0.249776	0.062388
MB_R_2091_19_10	0.719876	0.852263	0.250722	0.062861
MB_R_2091_19_30	0.690346	0.796855	0.269587	0.072677
MB_R_2091_19_10HQ	0.701567	0.819789	0.265490	0.070485
MB_R_2091_19_30HQ	0.704656	0.824439	0.261018	0.068131
MB_R_2091_19_EVA	0.766230	0.859049	0.196581	0.038644
MB_R_2091_19_SPIDER	0.756238	0.846924	0.208403	0.043432
MB_R_3642_WAM	0.721946	0.855873	0.249776	0.062388
MB_R_3642_10	0.719876	0.852263	0.250722	0.062861
MB_R_3642_30	0.690346	0.796855	0.269587	0.072677
MB_R_3642_10HQ	0.701567	0.819789	0.265490	0.070485
MB_R_3642_30HQ	0.704656	0.824439	0.261018	0.068131
MB_R_3642_EVA_1Scan	0.774004	0.865386	0.195210	0.038107
MB_R_3642_EVA_6Scans	0.766230	0.859049	0.196581	0.038644
MB_R_3642_SPIDER	0.756238	0.846924	0.208403	0.043432

Mean ratio algorithm within the 'per face' quality indicators was computed with MeshLab.

Lavoué *et al.* 2012), a platform development environment based on the class 'Polyhedron' of the Computational Geometry Algorithms Library (CGAL), for processing and visualization of mesh and mesh sequences. As this software does not work with STL files, the meshes were first exported to OBJ in Meshlab. This metric, in its current version and with the default parameters, is not able to compute large files. As the digitized meshes do not present many topological distortions they were decimated to two million vertices, so that the metric could handle them (G. Lavoué, pers. comm. 2020) with the exception of the meshes created with the Artec scanners, which already had a lower resolution. The decimation was computed with MeshLab (Quadric Edge Collapse Decimation algorithm), retaining the default settings, but also preserving the boundary of the mesh (for non-watertight meshes), normals, topology and planar simplification. These settings will attempt to preserve the general topology of the mesh and shape of the triangles. Furthermore, the quality threshold was set to 1, the maximum value (the higher the value the harder MeshLab attempts to adhere to the original model's shape). The 3D meshes were opened in Space mode in pairs, then the MSDM2 metric was computed in 'symmetry' with three scales. As a result of this symmetrical characteristic of the MSDM2, no mesh is defined as a reference. But, as previously noted, this metric needs to be calibrated. The best way to do this is by either comparing the meshes with the highest quality and using the MSDM2 score as a threshold of acceptance, or by 3D printing the mesh chosen as gold-standard, digitizing it, then comparing both meshes (G. Lavoué, pers. comm. 2020). In our case, we compared the chosen reference (digitized) mesh (see below) with its edited (without errors or holes) one for obtaining this threshold MSDM2 score. This edited 3D model is highly similar to the digitized mesh, so its function is the same as when using the digitized 3D printed model. One of the libraries used in the MSDM2 code showed a problem with several meshes (i.e. the MB.R.2091.19 ones created with the Artec scanners, and all the MB.R.3642 meshes). After a long period of computation, the software showed 'nan' (not a number) as the result. This problem was solved by not using the 'symmetry' option and indicating one of the meshes as a reference. For this, the reference mesh was opened first in the platform MEPP, and later the compared one was opened and added (in Space mode). The MSDM2 distance was then computed choosing '1 to 2' and three scales (the computation time will be longer, but the score is more accurate than with fewer scales) (G. Lavoué, pers. comm. 2020). The MSDM2 values are detailed in Table 5.

QUANTITATIVE AND TOPOLOGICAL COMPARATIVE ANALYSES

For comparing the STL files we used the software CloudCompare v.2.10-alpha (http://www.cloudcompare.org). The meshes were compared in pairs, using one as a reference (see below). First, both meshes were aligned; then the C2M algorithm was computed. It is important to note that this process is generally not symmetrical because the distances are 'orthogonal' to the surface of the reference mesh, and the meshes do not have exactly the same surface. As a result of this, it is important to remain consistent with the meshes considered as reference and the ones that are

TABLE 4. Specifications (number of photographs, accuracy and resolution), surface area and volume of each digitized and edited mesh.

3D model file name	STL		No. photos/ scans	Accuracy/ scaling error (m)	Resolution (no. vertices)	Mesh surface area (m^2)	Mesh volume (m^3)	Resolution of edited meshes	Edited mesh surface area (m^2)	Edited mesh volume (m^3)	Surface difference (m^2)	Difference in no. vertices	% Difference in no. vertices
	Faces	Size (MB)											
MB_R_2091_19_WAM	17 727 228	845 (ASCII)	237	0.000098	8 863 614	0.130819	0.001974	8 524 425	0.13423	0.001974	0.003411	−339 189	−3.83
MB_R_2091_19_10	16 892 773	805 (ASCII)	229	0.000198	8 446 476	0.136588	–	8 125 739	0.137391	0.001989	0.000803	−320 737	−3.80
MB_R_2091_19_30	16 897 708	805 (ASCII)	88	0.00004	8 448 987	0.135612	–	8 053 885	0.135975	0.001995	0.000363	−395 102	−4.68
MB_R_2091_19_10HQ	33 320 856	1.5GB (ASCII)	191	0.000177	16 660 749	0.126756	–	15 960 318	0.126658	0.001957	−0.000098	−700 431	−4.20
MB_R_2091_19_30HQ	31 079 777	1.44GB (ASCII)	71	0.000344	15 540 225	0.129134	–	14 889 591	0.129014	–	−0.000120	−650 634	−4.19
MB_R_2091_19_EVA	1 333 057	63.5 (ASCII)	10	0.00024	668 792	0.129623	–	695 497	0.13199	0.002028	0.002367	26 705	3.99
MB_R_2091_19_SPIDER	1 371 303	65.3 (ASCII)	18	0.00022	687 418	0.130528	–	725 023	0.133045	0.002029	0.002517	37 605	5.47
Mean surface and volume						0.131294	–		0.132615	0.001995	0.001320		
Cropped meshes													
MB_R_3642_WAM	8 840 258	421 (binary)	115	0.000073	4 424 093	0.032229	–	4 288 185	0.032264	–	0.032264	135 908	3.07
MB_R_3642_10	4 355 870	207 (binary)	113	0.000067	2 180 816	0.030506	–	2 114 615	0.030521	–	0.030521	66 201	3.04
MB_R_3642_30	4 170 984	198 (binary)	41	0.000085	2 088 062	0.030909	–	2 024 891	0.030942	–	0.030942	63 171	3.03
MB_R_3642_10HQ	10 747 600	512 (binary)	113	0.000071	5 378 063	0.030953	–	5 214 694	0.030974	–	0.030974	163 369	3.04
MB_R_3642_30HQ	10 231 868	487 (binary)	41	0.000044	5 120 176	0.031768	–	4 965 299	0.031796	–	0.031796	154 877	3.02
MB_R_3642_EVA_1Scan	319 901	15.2 (binary)	1	0.0002	160 816	0.031414	–	159 684	0.031414	–	0.031414	1132	0.70
MB_R_3642_EVA_6Scans	317 168	15.1 (binary)	6	0.00058	159 476	0.031321	–	158 394	0.031321	–	0.031321	1082	0.68
MB_R_3642_SPIDER	319 167	15.2 (binary)	5	0.00038	160 680	0.033796	–	159 714	0.033795	–	0.033795	966	0.60
Mean surface and volume						0.031612			0.031628		0.031628		

TABLE 5. MSDM2 scores, using MB.R.2091.19 WAM and MB.3642 TT30HQ meshes as references.

	MSDM2 score
MB.R.2091.19 WAM as reference	
D_E	0.05206
TT10	0.59947
TT30	0.59805
TT10HQ	0.60415
TT30HQ	0.61354
EVA	0.33868
SPIDER	0.33502
MB.R.3642 TT30HQ as reference	
D_E	0.02222
WAM	0.77955
TT10	0.78148
TT30	0.73978
TT10HQ	0.7153
EVA_1Scan	0.73572
EVA_6Scans	0.73613
SPIDER	0.69733

Note that the first value of each set (D_E) is the threshold score, computed between the digitized and edited meshes of each reference 3D model.

TABLE 6. 'Cloud-to-mesh distances' (C2M) values comparing the edited (E) (used as reference) and digitized (D) meshes.

	E (ref) vs D	Mean distance (m)	Standard deviation (m)
MB.R.2091.19	WAM	0	0.000004
	TT10	0	0.000007
	TT30	0	0.000015
	TT10HQ	0	0.000017
	TT30HQ	0	0.000021
	EVA	0.000022	0.000394
	SPIDER	−0.000019	0.000379
MB.R.3642	WAM	0	0.000004
	TT10	0	0.000004
	TT30	0	0.000003
	TT10HQ	0	0.000004
	TT30HQ	0	0.000003
	EVA_1Scan	0	0.000004
	EVA_6Scans	0	0.000034
	SPIDER	0	0.000029

Note that these C2M computations are asymmetrical, so one mesh must be taken as reference.

TABLE 7. 'Cloud-to-mesh distances' (C2M) values comparing the meshes chosen as reference (MB_R_2091_19_WAM and MB_R_3642_TT30HQ) with the others.

	Mean distance (m)	Standard deviation (m)
MB.R.2091.19 C2M with WAM as reference		
TT10	0.000071	0.000237
TT30	0.000053	0.000242
TT10HQ	−0.000262	0.000462
TT30HQ	0.000246	0.000362
EVA	0.000114	0.000205
SPIDER	0.000106	0.000209
WAM	0.000008	0.000403
MBR.3642 C2M with TT30HQ as reference		
TT10	0.000005	0.000160
TT30	0.000004	0.000303
TT10HQ	0.000002	0.000199
EVA_1Scan	−0.00001	0.000366
EVA_6Scans	0	0.000304
SPIDER	0.00001	0.000406

Note that these C2M computations are asymmetrical, so one mesh must be taken as reference.

compared with it. Default settings were used for distance computation. The mean distance and standard deviation values were saved for each quantitative comparison (Tables 6, 7), as well as the colour-grading images that visually display the distances between both meshes (Figs 4, 5). The colour scale indicates the distances between the triangles of each mesh, and has the same units as the created meshes (metres in this case). Warmer colours indicate that the compared mesh stands out from the reference one, while cooler colours indicate that the triangles of the compared mesh are inside the reference one. Similar meshes will present 'greenish' tonalities.

RESULTS

3D mesh errors

MB.R.2091.19. The meshes with fewer erroneous triangles were the ones created with the Artec scanners (a mean of 0.55% when compared with the total number of faces vs a mean of 2.99% for the meshes created by photogrammetry). In these cases, the protocol was highly automated, and the user could interfere less than with the other photogrammetric methods. However, more holes, sewing errors and erratic points were obtained using the structured light 3D scanners. The meshes with more errors were the ones created by photogrammetry with the turntable and the better quality camera equipment. This is also because the neural canal was not properly captured with this method, and it should be closed as if it was a hole. The mesh with fewest errors (excluding the number of intersections) was the one created with the

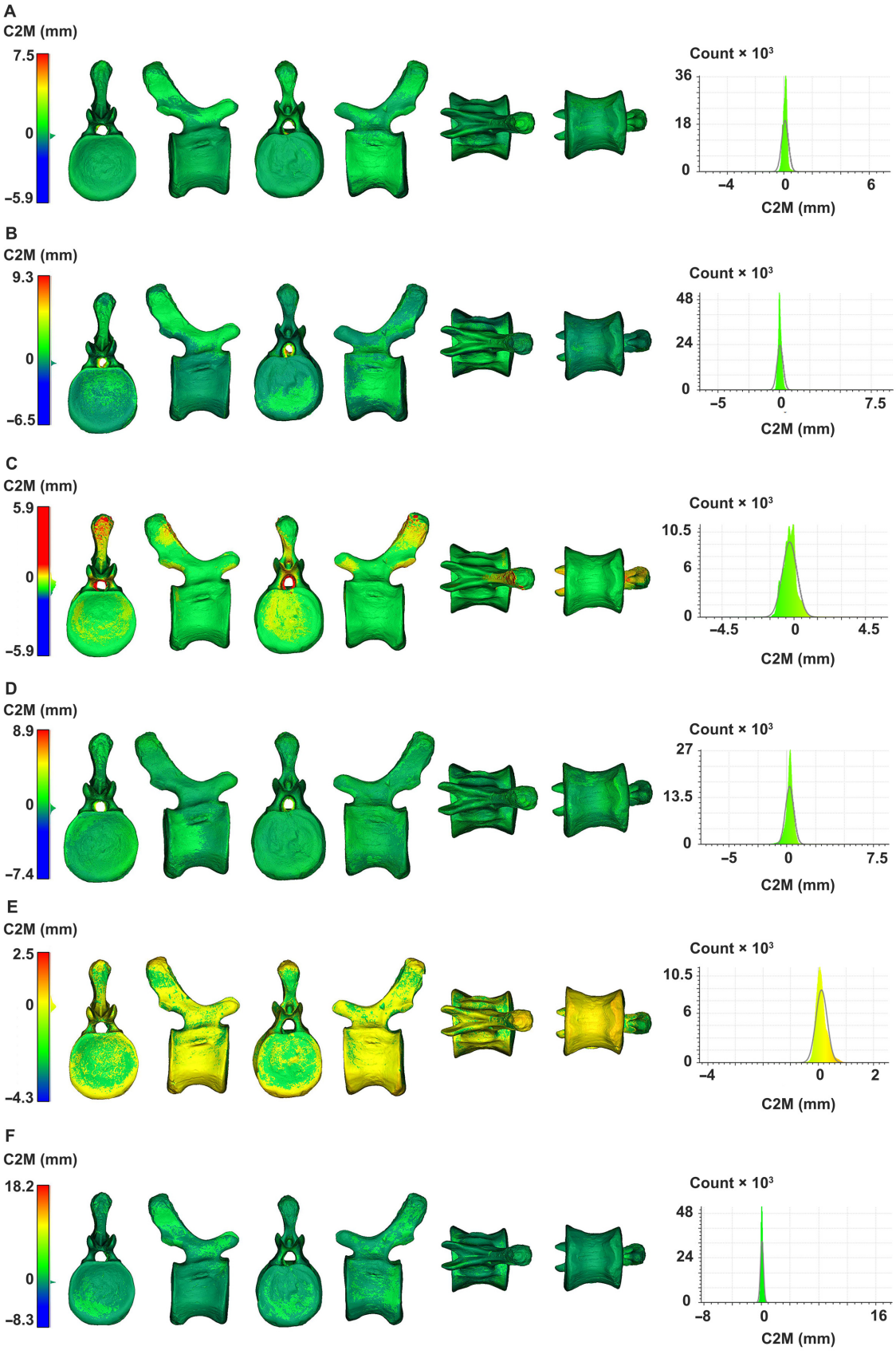
A
C2M (mm)
7.5
0
−5.9
Count × 10³
36
18
0
−4
0
6
C2M (mm)
B
C2M (mm)
9.3
0
−6.5
Count × 10³
48
24
0
−5
0
7.5
C2M (mm)
C
C2M (mm)
5.9
0
−5.9
Count × 10³
10.5
6
0
−4.5
0
4.5
C2M (mm)
D
C2M (mm)
8.9
0
−7.4
Count × 10³
27
13.5
0
−5
0
7.5
C2M (mm)
E
C2M (mm)
2.5
0
−4.3
Count × 10³
10.5
6
0
−4
0
2
C2M (mm)
F
C2M (mm)
18.2
0
−8.3
Count × 10³
48
24
0
−8
0
16
C2M (mm)

FIG 4. 'Cloud-to-mesh distances' (C2M) computed with CloudCompare using the MB.R.2091.19 mesh created by the 'walk-around method' (WAM) as reference and compared with: A, TT10 mesh; B, TT10HQ mesh,; C, TT30 mesh; D, TT30HQ mesh; E, Artec Eva scanner mesh; F, Artec Space Spider scanner mesh. Colour scale is in mm. Gaussian distribution histogram of each comparison included on the right.

photogrammetry WAM. It is interesting to note that only the TT10HQ mesh presented non-manifold edges, and both meshes created with the Artec scanners showed non-manifold vertices, all of them on the non-digitized zones of the neural canal.

MB.R.3642. The meshes created by photogrammetry presented more holes than the MB.R.2091.19 ones made using the same technique. However, one of these holes was present because the ventral surface of the specimen was not digitized. The Artec scanners created meshes with more holes, probably because of the difficulty in scanning flat surfaces with little relief (several holes are present in the girdles of the specimen). However, these meshes generally presented similar or fewer errors than the ones made by photogrammetry; for example, sewing errors, intersections, fanfolded triangles and number of degenerated triangles (a mean of 0.65% when compared with the total number of faces vs a mean of 2.13% for the meshes created by photogrammetry).

Mesh surface areas and volumes

Mesh surface area and volume were calculated with MeshLab for both the digitized and edited (after eliminating the errors and closing the holes) meshes (Table 4).

MB.R.2091.19. It was only possible to calculate the volume of the digitized meshes for the one created using the WAM (it being the only one without holes), as the others were not watertight (generally meshes consisting in one closed surface). The meshes with surface areas more similar to the calculated means were the ones created with the WAM and the Artec Space Spider for the digitized meshes, and both of the edited meshes created after both Artec scanners. Edited meshes with volume calculations more similar to the mean were the TT10 and TT30 ones. The meshes created with the photogrammetry WAM and TT10 showed fewer differences between the number of vertices between the digitized and the edited meshes (3.8% in relation to the digitized mesh).

MB.R.3642. The digitized and edited TT30HQ meshes were the ones with the most similar surface areas to their corresponding calculated means. The mesh created by the Artec Space Spider scanner had a higher surface area value, but also the lowest difference in number of vertices between the edited and the digitized meshes.

Choice of reference mesh for the comparative analyses

MB.R.2091.19. Taking into account all the information provided above, we chose the mesh created with the photogrammetry WAM as reference (with the highest quality) for the comparative analyses. This digitized mesh was the only one that was watertight (i.e. no holes were created in the process), it presented an accuracy (scaling error) of 0.000098 m, a high resolution (*c.* 8.8 million vertices), the lowest difference value (3.8%) between the number of vertices of the digitized and edited meshes were calculated for this method (i.e. the number and type of errors present in the digitized mesh did not influence the final quality of the 3D model as much as in the other meshes), non-manifold parts were absent, and the mesh surface area and volume values (for both digitized and edited meshes) were close to the calculated means. Furthermore, this mesh presented a high quality of triangulation (Fig. 6A, Table 3); computing values with the Mean Ratio algorithm revealed that most of the triangles of the mesh were close to being equilateral (shown in blue on the mesh and the histogram). However, most of the meshes created in this work presented good qualities of triangulation (Fig. 6).

To confirm this hypothesis, we also used CloudCompare to compare all the edited meshes with the digitized ones from which they originated (Table 6). The objective was to check whether the lower quality digitized meshes presented similar topologies to the edited ones (with no holes or errors). In these geometric comparisons, the edited meshes were considered to be reference. The obtained values confirmed the higher quality of the digitized mesh created with the WAM: a mean distance of 0 m, and a standard deviation of 0.000004 m indicate that this mesh is almost identical to the edited one. Good values were also obtained for the other photogrammetry methods, while the 3D models created with the Artec scanners showed more topological differences between both digitized and edited meshes.

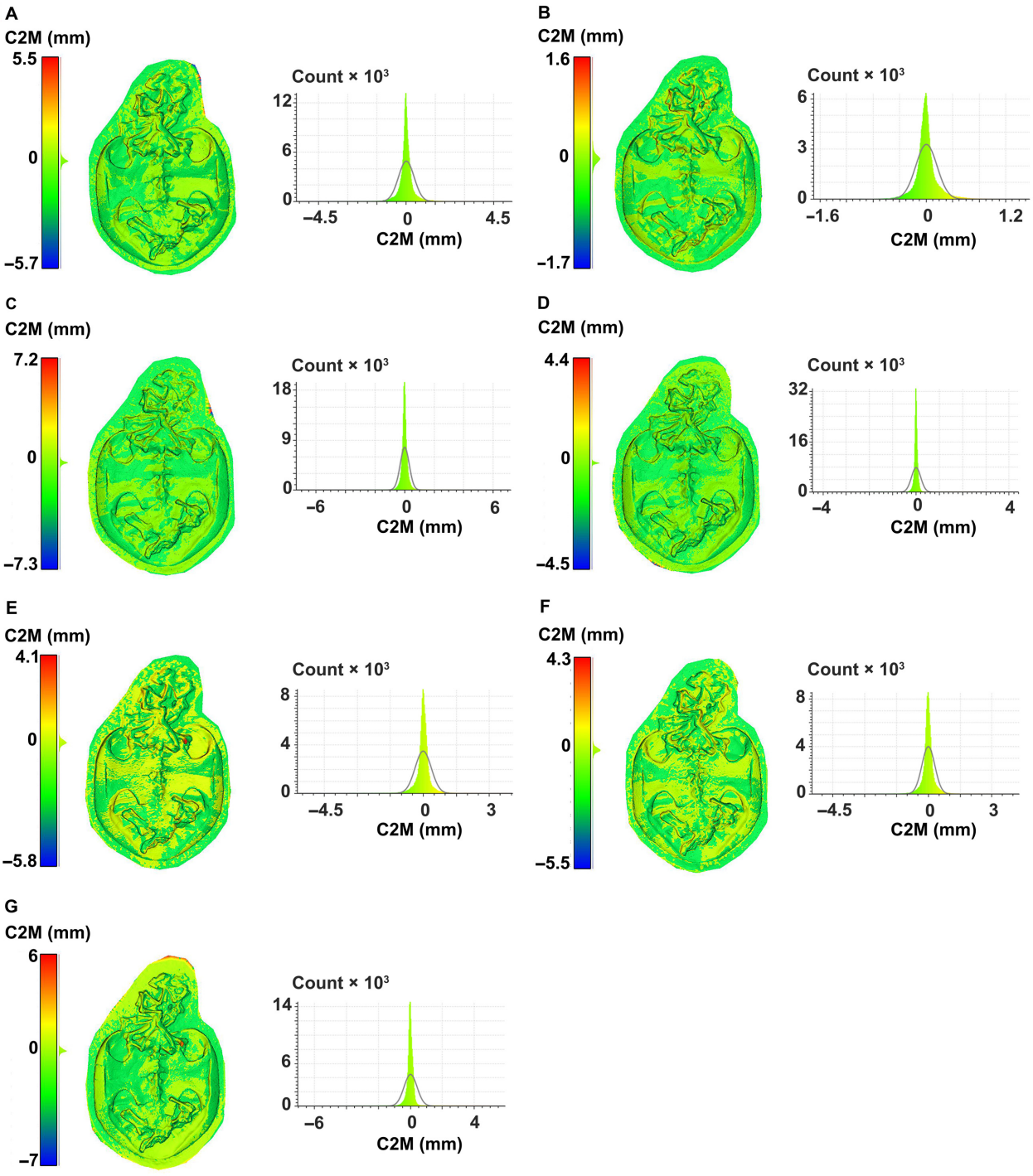

FIG 5. 'Cloud-to-mesh distances' (C2M) computed with CloudCompare using the MB.R.3642 TT30HQ mesh as reference and compared with: A, WAM mesh; B, TT10 mesh; C, TT30 mesh; D, TT10HQ mesh; E, Artec Eva scanner mesh (1 scan); F, Artec Eva scanner mesh (6 scans); G, Artec Space Spider scanner mesh. Colour scale is in mm. Gaussian distribution histogram of each comparison included on the right.

MB.R.3642. The choice for the MB.R.3642 reference mesh is more difficult to make, as all the 3D models presented similar qualities. The lowest scale error (accuracy) was calculated for the TT30HQ mesh (0.000044 m); it also presented a high resolution (*c.* 5 million vertices) and only two holes; non-manifold parts were absent.

However, the lowest difference in number of vertices between edited and digitized meshes was calculated for the Spider mesh (0.6%), meaning that this mesh was the most similar to its best version, and generally presented low error values. The quality of triangulation is good in all meshes, with the exception of the ones created by the Artec Eva scanner (Fig. 7 and Table 3).

'Cloud-to-mesh distances' between the edited and digitized meshes were also computed with CloudCompare to help in assessing the best 3D model (Table 6). In all of them, the mean distance was 0 m, while the lowest standard deviation values were found for the TT30 and TT30HQ meshes (0.000003 m).

As seen, all techniques produced good quality meshes for specimen MB.R.3642, especially the ones created by photogrammetry with the turntable (30°), the Canon EOS 5DS R DSLR camera and the Artec Space Spider scanner. For the next stage of comparisons we chose the TT30HQ mesh as a reference.

Objective mesh visual quality results

As previously stated, the MSDM2 metric is computed for paired 3D meshes (as OBJ files). The scores are indicated in Table 5. If the value is close to 0 then both meshes are approximately equal, and the closer the score approaches 1, the more differences (or visual distortions) exist between them. It is important to note that these scores are non-linear and cannot be interpreted as percentages. Firstly, a MSDM2 score as a threshold of acceptance was computed between the digitized mesh chosen as a reference and its edited (no errors or holes) mesh.

MB.R.2091.19. The MSDM2 score as a threshold of acceptance was computed between the digitized and edited WAM meshes, obtaining a value of 0.05206.

The mean score was 0.45, which indicates that all meshes presented visual differences from the one chosen as a reference. However, the lowest values were computed for the meshes created with the Artec scanners (*c.* 0.34), meaning that these 3D models were visually more similar to the mesh created by the photogrammetric WAM than the other meshes created by photogrammetry.

MB.R.3642. The MSDM2 score as a threshold of acceptance was computed between the digitized and edited TT30HQ meshes, obtaining a value of 0.02222. Although this value was lower than the one calculated for MB.R.2091.19, the rest of the MSDM2 scores were higher (mean of 0.74), meaning that visual differences were more perceptible between the MB.R.3642 meshes.

CloudCompare C2M quantitative comparisons

MB.R.2091.19. As previously noted, the mesh created by the photogrammetric WAM was used as a reference for the C2M quantitative comparisons (Table 7). The lowest mean distance scores (<0.1 mm) were computed for the meshes produced by photogrammetry with the Canon EOS 70D DSLR camera and the turntable. It is interesting to highlight that the highest mean distance and standard deviation scores were computed for the quantitative comparisons with the Canon EOS 5DS R DSLR camera and the turntable (10°). Indeed, it is interesting to check this less homogenized Gaussian distribution and topological distribution of the distance differences between meshes: they are more noticeable on the neural canal, neural spine and zygapophyses. As stated in Processing Protocols, above, the alignment of the photographs was problematic for the neural arch.

MB.R.3642. Mean distance values were lower than those calculated for the MB.B.2091.19 specimen (Table 7). However, standard deviation scores were generally similar to those. The lowest mean distance values were computed between the TT30HQ mesh chosen as reference and the mesh created with the Artec Eva Scanner (6 scans). Highest scores were computed for the Eva (1 scan) and Artec Space Spider scanners (0.01 mm), however, this could be related to one specific change that occurred on the specimen between digitization procedures: a bone of MB.R.3642, in the left axillary notch, was prepared between the photogrammetric and the structured light 3D scanning (EVA_1Scan and SPIDER meshes) procedures (see next section).

Visual topological comparisons. C2M distances were also displayed as colour-scaled figures (Figs 4, 5). With these graphics we can also assess the problematic zones when digitizing a specimen, and keep them in mind for possible modifications and improvements of the final mesh. These problematic zones were mainly the neural spine and canal in MB.R.2091.19 (as previously seen in the post/process protocols, especially in the methods that used the turntable), but also the articular surfaces of the centrum in several cases. Something similar occurred in MB.R.3642, in which the problematic zones were focused in surfaces with more relief (i.e. cranial bones, axillar and inguinal notches, and peripherals). This happened as not all digitization devices have the same resolution, as seen for example in the Artec scanners. Depending on the method employed, the user will need to focus more or less on problematic surfaces (normally the ones with more relief, depth, rugosities etc.) As the 3D models used in this project have a high level of detail, tiny modifications can be

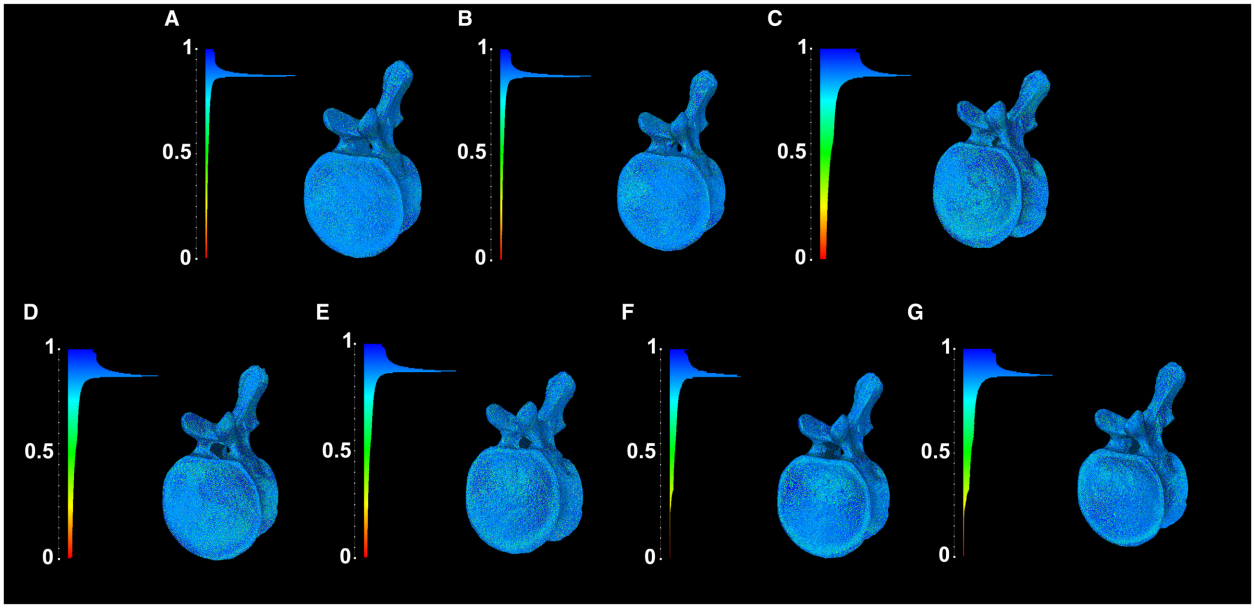

FIG 6. 'Per face' quality indicators (Mean Ratio algorithm) and histograms, computed with MeshLab, comparing edited and digitized meshes of MB.R.2091.19: A, WAM; B, TT10; C; TT30; D, TT10HQ; E, TT30HQ; F, Artec Eva scanner; G, Artec Space Spider scanner.

identified. The preparation of the piece of bone in the left axillary notch of MB.R.3642 can be noted in the comparisons with the Artec scanner meshes (Fig. 5E, G), presenting a difference of *c.* 4 mm between meshes in that zone (i.e. the bone fragment that has been prepared measures *c.* 4 mm).

DISCUSSION

The calculated mesh surface areas and volumes of the 3D meshes of the MB.R. 2091.19 specimen are highly similar (*c.* 0.13 m^2 and 0.0019 m^3) (Table 4). So, in general terms, we can confirm that accurate 3D models can be

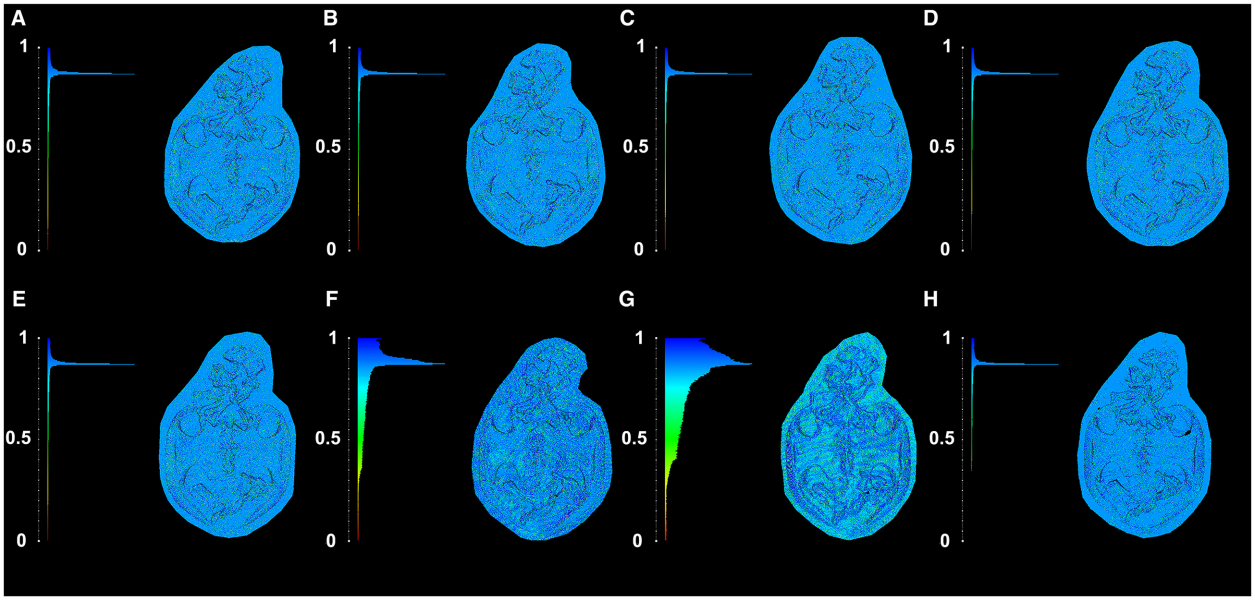

FIG 7. 'Per face' quality indicators (Mean Ratio algorithm) and histograms, computed with MeshLab, comparing edited and digitized meshes of MB.R.3642: A, WAM; B, TT10; C, TT30; D, TT10HQ; E, TT30HQ; F, Artec Eva scanner (1 scan); G, Artec Eva scanner (6 scans); H, Artec Space Spider scanner.

obtained with all seven of these different surface digitization methods and techniques, when relying on area and volume measurements. Sholts *et al.* (2010) also calculated the surface area and volumes of five human crania scanned with laser and white light scanners, and used these values for assessing the accuracy of the protocols and quality of the 3D models. They reported intraobserver measurement errors of 0.2% and interobserver errors of 2% of the total area and volume values. In our case, the surface and volume differences between meshes were of the submillimetre order (Table 4). Overall, surface area differences between meshes ranged from 0.2% to *c.* 5%, but some meshes presented higher scores (e.g. a 7.2% surface area difference was calculated between the TT10 and TT10HQ meshes). The lowest score difference (0.2%) was calculated between the WAM and SPIDER meshes. Regarding the number of photographs, we can observe that working in a range of 70–237 photographs for specimens like a vertebra with a simple neural spine (i.e. not having complex laminae or fossae patterns), a height of *c.* 30 cm and a centrum length of *c.* 10 cm can produce high quality surface 3D models. This helps us to confirm that the number of photographs (taking into account the minimum) is not important for the creation of an accurate 3D model; their quality and degree of overlap being more important, as well as the focus on more complex structures. However, when moving closer to the specimen, more details will be captured (i.e. a more accurate model will be created), but more photographs will be needed (Mallison & Wings 2014). The objective is to take an adequate number of photographs, so that each point of the specimen is well represented in sufficient detail in at least two additional images. In our case, we propose between *c.* 70 and 240 photographs when working with fossils of these sizes and external features, but the final number will ultimately be dependent on the user, device and specimen (see e.g. Fahlke & Autenrieth 2016, table 1; the number of photographs taken for the same specimen varies greatly, depending on the user who collected the data and the camera equipment employed). Indeed, the number of photographs required varies according to the complexity of the specimen and to the final resolution required of the digital model (Falkingham 2012).

It is important to remember that in our case the TT10HQ and TT30HQ did not correctly capture some surfaces of the specimen (i.e. the neural canal), which probably interfered with the final quality of the meshes and their perceptual metrics. This is because of the smaller depth of field of the Canon EOS 5DS R DSLR camera, which led to more problems in terms of focus and posterior calculation of points in the photogrammetry software (as seen in the difficulties when aligning the photographs). However, this did not happen with MB.R.3642 when digitized with the turntable and the Canon EOS 5DS R DSLR camera, but mainly because it is an almost entirely flat specimen with little relief, and the photographs probably had more (focused) surface overlap between them. So, when digitizing 'three-dimensional' specimens, it is better to use a camera with a large depth of field, or calculate and improve it with the camera specifications (e.g. lens aperture). We obtained high quality meshes of MB.R.3642 working with 40–110 photographs. As happened with the MB.R.2091.19 meshes, all the calculated surfaces were highly similar (*c.* 0.032 m^2) for the MB.R.3642 3D models (Table 4). Surface area differences between meshes ranged between *c.* 0.1% and 3% in most of them. However, the mesh created with the Artec Space Spider scanner showed higher differences percentages when compared with the other meshes, especially with the TT10 (9.73%) and TT30 (8.54%) meshes. The resolution (number of vertices) is more dependent on the resolution of the camera than on the number of photographs (e.g. see the resolutions of the MB.R.2091.19 WAM (237 photographs) and the TT30HQ (71 photographs) meshes: 8 863 614 faces vs 15 540 225 faces). The resolution of the mesh does not change dramatically when using the same camera equipment but fewer photographs (e.g. see the resolutions of the TT10HQ (191 photographs) and TT30HQ (71 photographs) meshes: 16 660 749 faces vs 15 540 225 faces).

With regard to the Artec scanners, we have seen that the resolution (number of vertices) of the meshes is between 10 and almost 25 times lower for both meshes when compared with the resolution of the meshes created by photogrammetry (Table 4), and more holes and erratic points are present (Table 2). However, these meshes presented lower values of degenerated triangles. The resolution of the meshes created by both Artec scanners is not greatly different, and the type and number of errors seems to be dependent on the scanner, the protocol (e.g. number, surface area, position of the scans) and external features. Regarding the number of scans, the mesh created with six scans with the Artec Eva scanner does present better quality indicators than the one created with only one scan, although these differences are not very appreciable. If the user is skilled enough, a good quality mesh can be created with this structured light 3D scanner by conducting only one scan, although we would advise scanning the specimen several times. However, specimens of the size and complexity of the ones digitized here do need to be scanned several times with the Artec Space Spider scanner due to the specifications of this device.

In our analyses and comparisons, we observed that the digitization technique that creates the comparatively highest quality meshes (i.e. smallest number of holes and errors, highest accuracy (lowest scaling error) and resolution, lowest mean distance and standard deviation values

between digitized and edited meshes) is photogrammetry. Taking into account all the values and comparisons obtained in this study, we designate the following cybertypes: MB.R.2091.19, the 3D model obtained by the photogrammetry WAM (MB_R_2091.19_WAM); MB.R.3642, the 3D model created by photogrammetry with the turntable (30°) and Canon EOS 5DS R camera equipment (MB_R_3642_TT30HQ) (see Figs 1, 2; https://doi.org/10.7479/khcz-ar29). These models show a high quality and level of detail, and also are highly similar to the physical specimen. The rest of the 3D models will be kept as digitypes.

However, an important issue should be noted in relation to the MB.R.3642 specimen and its cybertype. As indicated, the specimen was prepared between digitization techniques, so the chosen cybertype (MB_R_3642_TT30HQ) does not follow the first assumption of Faulwetter *et al.* (2013, p. 4) as it was digitized after this preparation: 'A cybertype should provide morphological and anatomical information of the same accuracy and reliability as provided by the physical type material...' The specimen was digitized with the Artec Space Spider scanner after the preparation work, but the quality of the mesh, although high, is not as good as the TT30HQ one. We do recommend digitizing the specimen when preparation work has been carried out, or even when the external features of the specimen have changed due to damage, so that the new cybertype follows the first assumption of Faulwetter *et al.* (2013). For assessing the quality of the new mesh we suggest following the quantitative comparison protocols of this study, using the old cybertype as a reference, so that the new cybertype at least has the same quality as the previous one. However, it is important to not delete previous cybertypes, so that the history of the changes and preparation work can be preserved and studied in the future. In summary, we consider the current cybertype MB_R_3642_TT30HQ to be provisional, until a 3D model with the actual external information of the MB.R.3642 specimen and with at least the same quality as the present mesh can be created.

Comparison of results with other works

Three previous studies have already compared 3D models created by photogrammetry and a well-known structured light 3D scanner: the Breuckmann stereoSCAN scanner, which has a diagonal scope of 250–720 mm, and a resolution of 18–22 μm (Katz & Friess 2014; Evin *et al.* 2016; Fau *et al.* 2016). The outputs created with the Breuckmann stereoSCAN scanner were considered as references in the comparisons with the meshes created by photogrammetry. These studies compared the models using visual qualitative and quantitative approaches (a geometric deviation map between the pairs of 3D models, and 3D landmark-based geometric morphometric analysis). However, the visual analyses relied on personal observations of the meshes (Evin *et al.* 2016), and, as has already been explained, these observations could be very subjective and their results depend on several factors. Using visual perceptual metrics for the visual qualitative comparisons provides more accurate and reliable results.

Katz & Friess (2014) indicated that the files originated by photogrammetry were larger than the ones created with the Breuckmann scanner. This is consistent with the results obtained here. Files created with the Artec scanners were between *c.* 12 and 33 times smaller, but also had a lower resolution (number of vertices) than the meshes created by photogrammetry.

The three studies obtained good quality 3D models with both photogrammetry and the Breuckmann scanner, with small differences in the geometry (below 0.5 mm (Evin *et al.* 2016) and 0.6 mm (Fau *et al.* 2016)) between meshes. In our analyses, we obtained differences in the geometry of 0.1 mm between the meshes created with the Artec scanners and the MB.R.2091.19 3D model created with the photogrammetric WAM, used as a reference in these geometric comparisons. In the case of MB.R.3642, the values were even lower, between 0 and 0.01 mm, for the comparison with the reference mesh TT30HQ. However, Katz & Friess (2014) suggested that meshes digitized using different techniques should not be mixed when working on analyses that rely on the detailed anatomy of the specimens, such as landmark placement and geometric morphometrics. Furthermore, the choice of the specific photogrammetry software could also influence the final quality of the mesh (Fau *et al.* 2016). We agree with Fau *et al.* (2016) that Agisoft PhotoScan (now known as Metashape) creates high quality meshes suitable for scientific study. However, following the results of this work, we advise caution when choosing 3D models created with the structured light 3D scanner as reference for the quantitative analyses and comparisons, as high quality meshes (even better than those from the scanner) can be obtained by photogrammetry.

CONCLUSION

Photogrammetry and structured light 3D scanners have been demonstrated to provide high quality surface 3D models when working with large specimens. Our results are in accordance with previous studies (Mallison & Wings 2014; Sutton *et al.* 2014; Fahlke & Autenrieth 2016; Fau *et al.* 2016), which concluded that the photogrammetry WAM (also known as manual photogrammetry) is among the most efficient surface digitization techniques for obtaining high quality 3D models of fossil

specimens. However, the structured light 3D scanners are the best option for inexperienced users, as it is a highly automated process. In addition, high quality 3D models can be created relatively quickly (for data acquisition as well as post/processing). 3D meshes can be created with only one scan, however, the final mesh will not have enough quality to be considered a cybertype. We suggest conducting a general scan of the specimen, then focusing on the details, using the Artec Eva or Space Spider scanners, depending on the size of the zone that needs to be scanned (scans from both scanners can be aligned later). As previously noted, a more accessible and affordable option is manual photogrammetry (depending on the software used). This method is recommended for more experienced users, as it is fast, and the user can focus on the most important features of the specimen. With a few properly taken photographs (depending on the size and complexity of the specimen to be digitized) a high quality 3D model can be obtained, but the post/processing effort and time could be higher than with structured light 3D scanning, depending on the desired final quality of the mesh. The camera does not need to be highly professional: we have demonstrated that cameras with fewer megapixels and a larger depth of field make the processing workflow easier, requiring less time to calculate the model. In addition, no special camera equipment (i.e. tripod and turntable) is required, which is important when the researcher needs to travel with photogrammetry equipment. We do recommend having a ring flash, proper and highly accurate scale bars and colourful fabrics in case they are needed for posterior masking of the background. In addition, we suggest as little as possible manual interference during the whole digitization process, in order to obtain the most similar 3D model to the physical specimen, so that it can be considered to be a cybertype.

Besides assessing several surface digitization techniques for vertebrate palaeontological specimens, we also suggest some quantitative, topological and visual comparison methods (i.e. distance computations and visual perceptual metrics) that help to better evaluate the quality of the created 3D meshes, and choose the most appropriate method for subsequent projects or the best model to be designated as the cybertype. Distance computations between meshes have previously been used for comparisons between digitized fossils; however, and though widely used in computer graphics, visual perceptual metrics have here been calculated and used for mesh comparisons for the first time for vertebrate palaeontological specimens. These metrics are useful for evaluating the objective visual quality of a 3D model, especially when the detailed anatomy of the specimen is needed; for example, for 3D musculoskeletal reconstructions, biomechanical analyses, landmark positioning, detailed anatomical descriptions and phylogenetic analyses when it is not possible to access the physical fossil, digitization of type or unique specimens.

We also recommend including within the essential and recommended files and data of each 3D model, a list of quality indicators, at least: the resolution (number of vertices), accuracy (scaling error), quality of triangulation, and presence/absence of topological artefacts (e.g. holes and non-manifold parts) (G. Lavoué & J. Marcé-Nogué, pers. comm. 2020). With this information, a better assessment of the quality of the mesh can be made by the creators of the 3D model and the researchers that will afterwards work with it or with similar quality meshes.

Acknowledgements. We would like to thank M. Belvedere (Università degli Studi di Firenze, Italy), B. Schurian and K. Mahlow (Museum für Naturkunde Berlin, Germany), E. Frey (Naturkundemuseum Karlsruhe, Germany), A. Pérez-García and D. Vidal (UNED, Madrid, Spain), J. Marcé-Nogué (Universitat Rovira i Virgili, Tarragona, Spain), G. Lavoué (LIRIS, INSA de Lyon, France) and D. Girardeau-Montaut (CloudCompare, France) for their invaluable help and comments, that greatly helped in the development of this work. J. Liston (Royal Tyrrell Museum of Palaeontology, Drumheller, Canada) kindly reviewed the English of the manuscript. We would like to thank S. Lautenschlager, S. Thomas, B. Lomax, I. Rahman and an anonymous reviewer for their useful comments and suggestions, which greatly improved the first drafts of this manuscript. This project is funded by the Berliner Hochschulprogramm für Wissenschaftlerinnen und Künstlerinnen, DiGiTal – Digitalisierung: Gestaltung und Transformation'. AB is supported by the Xunta de Galicia, Spain (ED481B 2017/027).

Author contributions. VDD and HM conceived and designed the study and tests. VDD digitized the specimens by surface methods, and created the 3D files and related data. VDD performed the comparisons and computed the metrics, interpreted the data, wrote the manuscript and prepared the figures. HM, PA, DS and AB read, commented and improved previous versions of the manuscript, and approved the submitted version.

DATA ARCHIVING STATEMENT

All created files and 3D models in this study are stored under CC-BY-NC license at the custodial three-dimensional repository of the Museum für Naturkunde Berlin (Germany): https://doi.org/10.7479/khcz-ar29

Editor. Imran Rahman

REFERENCES

ADAMS, T. L., STRGANAC, C., POLCYN, M. J. and JACOBS, L. L. 2010. High resolution three-dimensional

laser-scanning of the type specimen of *Eubrontes* (?) *glenrosensis* shuler, 1935, from the Comanchean (Lower Cretaceous) of Texas: implications for digital archiving and preservation. *Palaeontologia Electronica*, **13** (3), 1T, 11 pp.

AKKARI, N., ENGHOFF, H. and METSCHER, B. D. 2015. A new dimension in documenting new species: high-detail imaging for myriapod taxonomy and first 3D cybertype of a new millipede species (Diplopoda, Julida, Julidae). *PLoS One*, **10** (8), e0135243.

BALTSAVIAS, E. P. 1999. A comparison between photogrammetry and laser scanning. *ISPRS Journal of Photogrammetry & Remote Sensing*, **54** (2–3), 83–94.

BASTIR, M., GARCÍA-MARTÍNEZ, D., TORRES-TAMAYO, N., PALANCAR, C. A., FERNÁNDEZ-PÉREZ, F. J., RIESCO-LÓPEZ, A., OSBORNE-MÁRQUEZ, P., ÁVILA, M. and LÓPEZ-GALLO, P. 2019. Workflows in a virtual morphology lab: 3D scanning, measuring, and printing. *Journal of Anthropological Sciences*, **97**, 1–28.

BATES, K. T., RARITY, F., MANNING, P. L., HODGETTS, D., VILA, B., OMS, O., GALOBART, À. and GAWTHORPE, R. L. 2008. High-resolution LiDAR and photogrammetric survey of the Fumanya dinosaur tracksites (Catalonia): implications for the conservation and interpretation of geological heritage sites. *Journal of the Geological Society*, **165** (1), 115–127.

—— BREITHAUPT, B. H., FALKINGHAM, P. L., MATTHEWS, N. A., HODGETTS, D. and MANNING, P. L. 2009. Integrated LiDAR & photogrammetric documentation of the Red Gulch dinosaur tracksite (Wyoming, USA). 101–103. *In* FOSS, S. E., CAVIN, J. L., BROWN, T., KIRKLAND, J. I. and SANTUCCI, V. L. (eds). *Proceedings of the eighth conference on fossil resources*. St George, UT.

BERQUIST, R. M., GLEDHILLL, K. M., PETERSON, M. W., DOAN, A. H., BAXTER, G. T., YOPAK, K. E., KANG, N., WALKER, H. J., HASTINGS, P. A. and FRANK, L. R. 2012. The digital fish library: using MRI to digitize, database, and document the morphological diversity of fish. *PLoS One* **7** (4), e34499.

BREITHAUPT, B. H., SOUTHWELL, E. H., ADAMS, T. and MATTHEWS, N. A. 2001. Innovative documentation methodologies in the study of the most extensive dinosaur tracksite in Wyoming. 113–122. *In* SANTUCCI, V. L. and McCLELLAND, L. (eds). *Proceedings of the 6th fossil research conference*. Geologic Resources Division Technical Report.

—— MATTHEWS, N. A. and NOBLE, T. A. 2004. An integrated approach to three-dimensional data collection at Dinosaur tracksites in the Rocky Mountain West. *Ichnos*, **11** (1), 11–26.

CERRONI, M. A., CANALE, J. I., NOVAS, F. E. and PAULINA-CARABAJAL, A. 2020. An exceptional neurovascular system in abelisaurid theropod skull: new evidence from *Skorpiovenator bustingorryi*. *Journal of Anatomy*, published online 22 June. https://doi.org/10.1111/joa.13258

CORSINI, M., LARABI, M. C., LAVOUÉ, G., PETRIK, O., VÁŠA, L. and WANG, K. 2012. Perceptual metrics for static and dynamic triangle meshes. *Computer Graphics Forum*, **32** (1), 101–125.

DAVIES, T. G., RAHMAN, I. A., LAUTENSCHLAGER, S., CUNNINGHAM, J. A., ASHER, R. J., BARRETT, P. M., BATES, K. T., BENGTSON, S., BENSON, R. B. J., BOYER, D. M., BRAGA, J., BRIGHT, J. A., CLAESSENS, L. P. A. M., COX, P. G., DONG, X.-P., EVANS, A. R., FALKINGHAM, P. L., FRIEDMAN, M., GARWOOD, R. J., GOSWAMI, A., HUTCHINSON, J. R., JEFFERY, N. S., JOHANSON, Z., LEBRUN, R., MARTÍNEZ-PÉREZ, C., MARUGÁN-LOBÓN, J., O'HIGGINS, P. M., METSCHER, B., ORLIAC, M., ROWE, T. B., RÜCKLIN, M., SÁNCHEZ-VILLAGRA, M. R., SHUBIN, N. H., SMITH, S. Y., STARCK, J. M., STRINGER, C., SUMMERS, A. P., SUTTON, M. D., WALSH, S. G. A., WEISBECKER, V., WITMER, L. M., WROE, S., YIN, Z., RAYFIELD, E. J. and DONOGHUE, P. C. J. 2017. Open data and digital morphology. *Proceedings of the Royal Society B*, **284**, 20170194.

DÍEZ DÍAZ, V., MALLISON, H., ASBACH, P., SCHWARZ, D. and BLANCO, A. 2020. Model: Digital files and supplementary information on the comparison between several digitization techniques and methods. *MfN Data Repository*. https://doi.org/10.7479/khcz-ar29

EVIN, A., SOUTER, T., HULME-BEAMAN, A., AMEEN, C., VIACAVA, M., LARSON, G., CUCCHI, T. and DOBNEY, K. 2016. The use of close-range photogrammetry in zooarchaeology: creating accurate 3D models of wolf crania to study dog domestication. *Journal of Archaeological Science*, **9**, 87–93.

FAHLKE, J. M. and AUTENRIETH, M. 2016. Photogrammetry vs. micro-ct scanning for 3D surface generation of a typical vertebrate fossil – a case study. *Journal of Paleontological Techniques*, **14**, 1–18.

FALKINGHAM, P. L. 2012. Acquisition of high resolution three-dimensional models using free, open-source, photogrammetric software. *Palaeontologia Electronica*, **15**, 15.

—— BATES, K. T., AVANZINI, M., BENNETT, M., BORDY, E. M., BREITHAUPT, B. H., CASTANERA, D., CITTON, P., DÍAZ-MARTÍNEZ, I., FARLOW, J. O., FIORILLO, A. R., GATESY, S. M., GETTY, P., HATALA, K. G., HORNUNG, J. J., HYATT, J. A., KLEIN, H., LALLENSACK, J. N., MARTIN, A. J., MARTY, D., MATTHEWS, N. A., MEYER, C. A., MILÀN, J., MINTER, N. J., RAZZOLINI, N. L., ROMILIO, A., SALISBURY, S. W., SCISCIO, L., TANAKA, I., WISEMAN, A. L. A., XING, L. D. and BELVEDERE, M. 2018. A standard protocol for documenting modern and fossil ichnological data. *Palaeontology*, **61** (4), 469–480.

FAU, M., CORNETTE, R. and HOUSSAYE, A. 2016. Photogrammetry for 3D digitizing bones of mounted skeletons: potential and limits. *Comptes Rendus Palevol*, **15**, 968–977.

FAULWETTER, S., VASILEIADOU, A., KOURATORAS, M., THANOS, D. and ARVANIDITIS, C. 2013. Micro-computed tomography: introducing new dimensions to taxonomy. *ZooKeys*, **263**, 1–45.

FENG, X., WAN, W., XU, R. Y. D., CHEN, H., PENGFEI, L. and SÁNCHEZ, J. A. 2018. A perceptual quality metric for 3D triangle meshes based on spatial pooling. *Frontiers of Computer Science*, **12**, 798–812.

GIACOMINI, G., SCARAVELLI, D., HERREL, A., VENEZIANO, A., RUSSO, D., BROWN, R. P. and MELORO, C. 2019. 3D photogrammetry of bat skulls: perspectives for macro-evolutionary analyses. *Evolutionary Biology*, **46** (3), 249–259.

GODFRAY, H. C. J. Jr 2007. Linnaeus in the information age. *Nature*, **446** (15), 259–260.

GONIZI BARSANTI, S. and GUIDI, G. 2013. 3D digitization of museum content within the 3D-ICONS project. *ISPRS Annals of the Photogrammetry, Remote Sensing & Spatial Information Sciences*, **II-5 W1**, 151–156.

HAMM, C. A., MALLISON, H., HAMPE, O., SCHWARZ, D., MEWS, J., BLOBEL, J., ISSEVER, A. S. and ASBACH, P. 2018. Efficiency, workflow and image quality of clinical computed tomography scanning compared to photogrammetry on the example of a *Tyrannosaurus rex* skull from the Maastrichtian of Montana, USA. *Journal of Paleontological Techniques*, **21**, 1–13.

HEUMANN, I., STOECKER, H., TAMBORINI, M. and VENNEN, M. 2018. *Dinosaurierfragmente: Zur Geschichte der Tendaguru-Expedition und ihrer Objekte, 1906–2018*. Wallstein Verlag.

IBRAHIM, N., MAGANUCO, S., DAL SASSO, C., FABBRI, M., AUDITORE, M., BINDELLINI, G., MARTILL, D. V., ZOUHRI, S., MATTARELLI, D. A., UNWIN, D. M., WIEMANN, J., BONADONNA, D., AMANE, A., JAKUBCZAK, J., JOGER, U., LAUDER, G. V. and PIERCE, S. E. 2020. Tail-propelled aquatic locomotion in a theropod dinosaur. *Nature*, **581** (7806), 67–70.

KATZ, D. and FRIESS, M. 2014. 3D from standard digital photography of human crania—a preliminary assessment. *American Journal of Physical Anthropology*, **154** (1), 152–158.

KNUPP, P. 2007. Remarks on mesh quality. *In 45th AIAA aerospace sciences meeting and exhibit*, Sandia National Laboratories.

LAUTENSCHLAGER, S. 2016. Reconstructing the past: methods and techniques for the digital restoration of fossils. *Royal Society Open Science*, **3**, 160342.

LAVOUÉ, G. 2011. A multiscale metric for 3D mesh visual quality assessment. *Computer Graphics Forum*, **30** (5), 1427–1437.

—— and CORSINI, M. 2010. A comparison of perceptually-based metrics for objective evaluation of geometry processing. *IEEE Transactions on Multimedia*, **12** (7), 636–649.

—— TOLA, M., DUPONT, F. 2012. **1**, MEPP – 3D Mesh Processing Platform. *Proceedings of the International Conference on Computer Graphics Theory & Applications (GRAPP)*, **1**, 206–210. https://doi.org/10.5220/0003928502060210

LINDSTROM, P. and TURK, G. 2000. Image-driven simplification. *ACM Transactions on Graphics*, **19** (3), 204–241.

MALLISON, H. 2010. The digital *Plateosaurus* II: an assessment of the range of motion of the limbs and vertebral column and of previous reconstructions using a digital skeletal mount. *Acta Palaeontologica Polonica*, **55** (3), 433–458.

—— and WINGS, O. 2014. Photogrammetry in paleontology – a practical guide. *Journal of Paleontological Techniques*, **12**, 1–31.

—— BELVEDERE, M. and DÍEZ DÍAZ, V. 2017. Photogrammetry MfN. *In 3D imaging handbook*. SYNTHESYS project, Museum für Naturkunde, Berlin. http://biowikifarm.net/v-mfn/3d-handbook/Photogrammetry_MfN [accessed 2019]

MANNION, P. D., UPCHURCH, P., SCHWARZ, D. and WINGS, O. 2019. Taxonomic affinities of the putative titanosaurs from the Late Jurassic Tendaguru formation of Tanzania: phylogenetic and biogeographic implications for eusauropod dinosaur evolution. *Zoological Journal of the Linnean Society*, **185** (3), 784–909.

MARCY, A. E., FRUCIANO, C., PHILLIPS, M. J., MARDON, K. and WEISBECKER, V. 2018. Low resolution scans can provide a sufficiently accurate, cost-and time-effective alternative to high resolution scans for 3D shape analyses. *PeerJ*, **6**, e5032.

MATTHEWS, N. A., NOBLE, T. and BREITHAUPT, B. 2006. The application of photogrammetry, remote sensing and geographic information systems (GIS) to fossil resource management. *Americas Antiquities: 100 Years of Managing Fossils on Federal Lands: Bulletin* **34** (34), 119.

MATTHEWS, N., NOBLE, T., BREITHAUPT, B. H., FALKINGHAM, P. L., MARTY, D. and RICHTER, A. 2016. Close-range photogrammetry for 3-D ichnology: the basics of photogrammetric ichnology. 29–55. *In* FALKINGHAM, P. L., MARTY, D. and RICHTER, A. (eds). *Dinosaur tracks: The next steps*. Indiana University Press.

MUÑOZ-MUÑOZ, F., QUINTO-SÁNCHEZ, M. and GONZÁLEZ-JOSÉ, R. 2016. Photogrammetry: a useful tool for three-dimensional morphometric analysis of small mammals. *Journal of Zoological Systematics & Evolutionary Research*, **54** (4), 318–325.

PETERSON, J. E. and KRIPPNER, M. L. 2019. Comparisons of fidelity in the digitization and 3D printing of vertebrate fossils. *Journal of Paleontological Techniques*, **22**, 1–19.

PRICE, L. I. 1973. Quelônio amphichelydia no Cretáceo inferior do nordeste do Brazil. *Revista Brasileira do Geociéncias*, **3**, 84–96.

RAMOS BARBERO, B. and SANTOS URETA, E. 2011. Comparative study of different digitization techniques and their accuracy. *Computer-Aided Design*, **43** (2), 188–206.

ROBINSON, C. and TERHUNE, C. E. 2017. Error in geometric morphometric data collection: combining data from multiple sources. *American Journal of Physical Anthropology*, **164** (1), 62–75.

ROGOWITZ, B.-E. and RUSHMEIER, H.-E. 2001. Are image quality metrics adequate to evaluate the quality of geometric objects? *Proceedings of Human Vision & Electronic Imaging*, 340–348.

SHOLTS, S. B., WÄRMLÄNDER, S. K., FLORES, L. M., MILLER, K. W. and WALKER, P. L. 2010. Variation in the measurement of cranial volume and surface area using 3D laser scanning technology. *Journal of Forensic Sciences*, **55 (4)**, 871–876.

SIVETER, D. J., BRIGGS, D. E., SIVETER, D. J. and SUTTON, M. D. 2020. The Herefordshire Lagerstätte: fleshing out Silurian marine life. *Journal of the Geological Society*, **177** (1), 1–13.

SLIZEWSKI, A., FRIESS, M. and SEMAL, P. 2010. Surface scanning of anthropological specimens: nominal-actual comparison with low cost laser scanner and high end fringe light projection surface scanning systems. *Quartär*, **57**, 179–187.

STOEV, P., KOMERIČKI, M. A., WÄRMLÄNDER, S. K. AKKARI, N., LIU, M. S.ZHOU, M. X., WEIGAND, A. M. HOSTENS, J., HUNTER, C. I.EDMUNDS, S. C., PORCO, D. ZAPPAROLI, M., GEORGIEV, T. MIETCHEN, D., ROBERTS, D.FAULWETTER, S., SMITH, V. and PENEV, L. 2013. Eupolybothrus cavernicolus Komerički & Stoev sp. n. (Chilopoda: Lithobiomorpha: Lithobiidae): the first eukaryotic species description combining transcriptomic, DNA barcoding and micro-CT imaging data. *Biodiversity Data Journal*, **1**, e1013.

SUTTON, M. D., BRIGGS, D. E., SIVETER, D. J. and SIVETER, D. J. 2001*a*. Methodologies for the visualization and reconstruction of three-dimensional fossils from the Silurian Herefordshire Lagerstätte. *Palaeontologia Electronica*, **4** (1), 1–17.

—— —— —— —— 2001*b*. A three-dimensionally preserved fossil polychaete worm from the Silurian of Herefordshire England. *Proceedings of the Royal Society B*, **268** (1483), 2355–2363.

—— RAHMAN, I. A. and GARWOOD, R. J. 2014. *Techniques for virtual palaeontology*. Wiley.

TSUBOI, M., KOPPERUD, B. T., SYROWATKA, C., GRABOWSKI, M., VOJE, K. L., PÉLABON, C. and HANSEN, T. F. 2020. Measuring complex morphological traits with 3D photogrammetry: a case study with deer antlers. *Evolutionary Biology*, **47**, 175–186.

VIDAL, D. and DÍEZ DÍAZ, V. 2017. Reconstructing hypothetical sauropod tails by means of 3D digitization: *Lirainosaurus astibiae* as case study. *Journal of Iberian Geology*, **43** (2), 293–305.

VIDAL, L. D. S., PEREIRA, P. V. L. G. D. C., TAVARES, S., BRUSATTE, S. L., BERGQVIST, L. P. and CANDEIRO, C. R. D. A. 2020. Investigating the enigmatic Aeolosaurini clade: the caudal biomechanics of *Aeolosaurus maximus* Aeolosaurini/Sauropoda) using the neutral pose method and the first case of protonic tail condition in Sauropoda. *Historical Biology*, published online 13 April. https://doi.org/10.1080/08912963.2020.1745791

WANDEL, B. A. 1995. *Foundations of vision*. Sinauer Associates, Sunderland, MA.

ZHU, Q., ZHAO, J., DU, Z. and ZHANG, Y. 2010. Quantitative analysis of discrete 3D geometrical detail levels based on perceptual metric. *Computers & Graphics*, **34** (1), 55–65.